Tunable Electronic Transport Properties of 2D Layered Double Hydroxide Crystalline Microsheets with Varied Chemical Compositions

Yibing Zhao, Hai Hu, Xiaoxia Yang,* Dongpeng Yan,* and Qing Dai*

Layered 2D atomic materials not only demonstrate novel and extraordinary properties in and of themselves,[1–3] but also function as useful heterostructures when arranged in stacked layers, as in tunneling diodes, tunneling transistors, light-emitting diodes, solar cells, and hybridized plasmon–phonon polaritons.[4–12] Increasing the amount and types of available 2D materials, as well as improving the quality of their electronics, will also increase the range of possible heterostructures and their functionalities. Existing 2D atomic crystals can be found in the form of conductors (e.g., graphene), insulators (e.g., h-BN), or semiconductors (e.g., transition metal dichalcogenides).[13–16] However, 2D ion monolayers have yet to be studied for use in functional ionic devices, such as batteries, fuel cells, (electro)chemical sensors, and electrochemical devices, all of which are increasingly useful technologies.[17,18]

2D layered double hydroxides (LDH) function as natural positively charged hosts for anions.[19–21] LDH consist of 2D brucite-like octahedral hydroxide layers that hold a positive charge due to a portion of the divalent metal cations (M^{2+}) being substituted by trivalent cations (M^{3+}). To achieve charge balance, anions travel through the material to an interlayer gallery.[19] The chemical composition of LDH is expressed by the general formula $M^{2+}_{1-x}M^{3+}_x(OH)_2A^{n-}_{x/n} \cdot mH_2O$, where $M^{2+} = Mg^{2+}$, Fe^{2+}, Co^{2+}, Ni^{2+}, Zn^{2+}, etc.; $M^{3+} = Al^{3+}$, Fe^{3+}, Co^{3+}, etc.; and $A^{n-} = CO_3^{2-}$, NO_3^-, Cl^-, ClO_4^-, or other organic functional molecules. The metal cations and interlayer anion types can be creatively tuned to have M^{2+}/M^{3+} molar ratios that result in a variety of host–guest assemblies with versatile properties.[22–25] LDH have been used as ion-exchange materials, catalysts, sorbents including halogen absorbers, bioactive nanocomposites, and electroactive and photoactive materials.[26–31] Detailed studies of the electrical properties of the LDH are required in order to fully understand the mechanics of these materials, especially those closely related with ion transport and charge activity. However, due to the limited size of individual LDH crystals as well as their tendency to form irregular aggregations, an electrical transport study has yet to be completed for a LDH single crystal.[32] Due to recent improvements in the synthesis of 2D LDH single crystals, crystals dozens of micrometers in size have been prepared,[26,33,34] a development which paves the way for an electrical transport study.

In this work, we fabricated field effect transistors based on LDH single crystals in order to study their electrical properties for the first time. Specifically, we studied the effects of various metal cations in the host layers ($M^{2+} = Mg^{2+}$ and Zn^{2+}, $M^{3+} = Al^{3+}$) and interlayer anions ($A^{n-} = CO_3^{2-}$ and NO_3^-) on LDH electrical properties. The electrical transport properties of ultrathin LDH layers that had been exfoliated from as-synthesized single crystals were also measured. Our results suggest that 2D LDH conductivity arises primarily from hole migration within the host layer, and has a carrier mobility of $\approx 9 \times 10^{-5}$ cm^2 V^{-1} s^{-1}. This conductivity can be largely tuned by the selection of metal cations as well as interlayer anions, while it can only be weakly tuned by the external electric field. Additionally, the conductivity was seen to decrease for a decrease in the thickness of the LDH layers. The results of this work give a fundamental and detailed understanding of the electrical transport properties of LDH for future electric, electrochemical, and electrocatalytic studies.

A modified coprecipitation method using urea as a precipitation agent was used to successfully synthesize $M^{II}Al$-CO_3-LDH ($M^{II} = Mg^{2+}$ or Zn^{2+}) microsheets (as shown in the Supporting Information).[35] LDH solids were dispersed in alcohol and then spin coated onto a SiO$_2$/Si substrate. A typical scanning electron microscope (SEM) image of MgAl-CO$_3$-LDH single crystals is shown in **Figure 1**a, and reveals a collection of hexagonal platelets with an average lateral length of 10 μm. By increasing the aging time (36 h), the crystal size was increased to roughly 20 μm (Figure S1a–c, Supporting Information). The morphologies of ZnAl-CO$_3$-LDH crystals were also observed to have a similar hexagonal

Y. Zhao, H. Hu, Dr. X. Yang, Prof. Q. Dai
National Center for Nanoscience and Technology
Beijing 100190, P. R. China
E-mail: yangxx@nanoctr.cn; daiq@nanoctr.cn

Y. Zhao, Prof. D. Yan
Key Laboratory of Theoretical and Computational Photochemistry
Ministry of Education
Beijing Key Laboratory of Energy Conversion and Storage Materials
College of Chemistry
Beijing Normal University
Beijing 100875, P. R. China
E-mail: yandp@bnu.edu.cn

Y. Zhao, Prof. D. Yan
State Key Laboratory of Chemical Resource Engineering
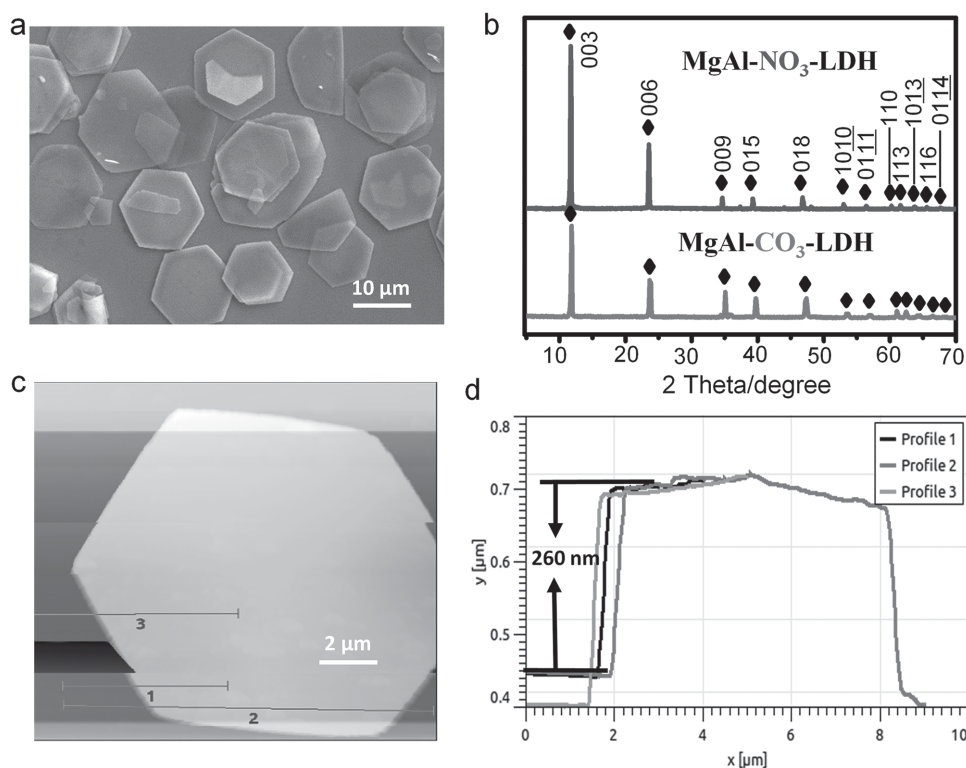Beijing University of Chemical Technology
Beijing 100029, China

Figure 1. a) SEM image of monodispersed hexagonal plate-like MgAl-CO₃-LDH microcrystals. b) XRD patterns of MgAl-CO₃-LDH and ZnAl-CO₃-LDH. c) AFM image of a typical LDH microsheet. d) AFM line profiles corresponding to lines show in (c).

platelet structure. X-ray diffraction (XRD) was used to demonstrate that both types of LDH contained high-quality crystals. As shown in Figure 1b, basal reflections in each XRD profile had *d* values of 0.75 and 0.375 nm and were assigned to the 003 and 006 reflections, respectively, a pattern common in LDH systems intercalated with the CO_3^{2-} anion. The peaks at ca. 39°, 47°, 56°, and 68° can be attributed to the (01*l*) reflections of MgAl-CO₃-LDH or ZnAl-CO₃-LDH, i.e., (015), (018), (0111), and (0114) reflections correspondingly. These reflections correspond to the rhombohedral symmetry stacking patterns of the MgAl-CO₃-LDH and ZnAl-CO₃-LDH host layers.[36] The peak at 62° can be attributed to the (110) reflection which determines the value of the lattice parameter *a* = 0.3063 nm of the MgAl-CO₃-LDH and ZnAl-CO₃-LDH by the equation $a = 2d_{(110)}$. The appearance of (1010) and (1013) reflections is due to typical brucite structure.[37] Furthermore, the peaks at 61° and 66° can be attributed to the (113) and (116) reflections of the MgAl-CO₃-LDH or ZnAl-CO₃-LDH host layers.[38] The sharp and symmetric features of the diffraction peaks strongly support a high degree of crystalline structure in the LDH samples. These results were further verified using transmission electron microscopy (TEM). Figure S1d (Supporting Information) shows an example of a typical TEM image and the corresponding selected area electron diffraction (SAED) image of an individual MgAl-CO₃-LDH platelet. The TEM profile revealed that the platelet does indeed have a uniform and smooth surface due to its 2D layered structure. The well-defined SAED pattern further confirms the single crystal characteristics in the LDH microplatelet. The electron diffraction pattern was indexed as the [00*l*] direction, and was in good agreement with the XRD patterns previously collected. Based on these results, the as-prepared $M^{II}Al$-CO₃-LDH microsheets were shown to be of high quality in terms of morphology, size, uniformity, and crystallinity.

The thickness and surface morphology of synthesized LDH microsheets were characterized using atomic force microscopy (AFM). Figure 1c shows a typical AFM image of an LDH crystal, and confirms that the surface is smooth, while Figure 1d shows the height to be ≈260 nm. The 2D hexagonal morphology of the LDH microcrystals can be attributed to their crystallographic nature and 3R rhombohedral symmetry.[19] The uniformity, large size, and high crystallinity of the crystals are a result of a slow and homogeneous nucleation process coupled with slow urea hydrolysis.[39] Furthermore, using the $M^{II}Al$-CO₃-LDH crystals, it is possible to obtain high quality $M^{II}Al$-NO₃-LDH crystals using an anion exchange process, specifically a salt–acid treatment method (shown in the Supporting Information).[40]

Using the as-obtained high-quality single crystalline LDH microsheets dispersed on SiO₂/Si, field effect transistors (FETs) were fabricated utilizing the LDH crystals as channels. **Figure 2**a shows a schematic of the transistor structure, which is an LDH single crystal connected by two Au electrodes acting as the source and drain all atop a highly doped Si gate. In order to synthesize these transistors, LDH crystals were first covered by a layer of poly(methyl methacrylate) (PMMA) patterned using electron beam lithography (EBL) to define the desired electrode patterns. The Au electrodes were then formed by depositing an Au film using electron beam evaporation followed by a liftoff procedure. Figure 2b shows a SEM image of a typical
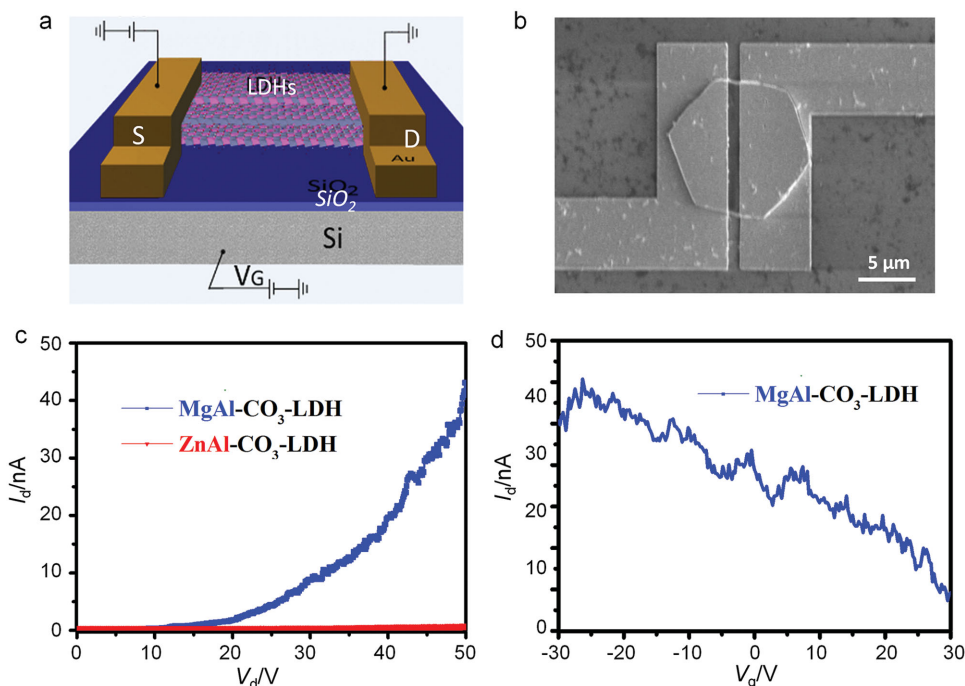
Figure 2. a) 3D schematic diagram of the fabricated field effect transistor device. b) SEM image of the fabricated FET device defined by two gold pads serving as source and drain electrodes for the microcrystal. c) I_d–V_d curves measured for the devices based on individual MgAl-CO$_3$-LDH and ZnAl-CO$_3$-LDH microcrystals, $V_g = 0$ V. d) I_d–V_g curve of the MgAl-CO$_3$-LDH device while experiencing a bias voltage, $V_d = 40$ V.

device based on a single MgAl-CO$_3$-LDH microcrystal. The channel width and length of the transistor were 8 and 1 μm, respectively.

The electrical properties of all of the fabricated devices were measured in a probe station under ambient conditions. Figure 2c shows the typical output characteristics [current (I)–drain voltage (V_d) curves] of the fabricated devices based on individual MgAl-CO$_3$-LDH and ZnAl-CO$_3$-LDH microcrystals. For both types of LDH based devices, the I_{ds} versus V_{ds} curves are strongly nonlinear, a result typical for semiconducting channels with Schottky barriers at the contacts. The electric conductivity of the MgAl-CO$_3$-LDH based device was measured to be much higher than that of the ZnAl-CO$_3$-LDH based transistor. For example, for an equal value of $V_d = 50$ V, the I_d value reached 43 nA for the MgAl-CO$_3$-LDH, but only 0.4 nA for ZnAl-CO$_3$-LDH. This difference in electric conductivity is due to the differing ionic radii and electronic structures of the intralayer metal cations, as well as the different degrees of distortion of the MO$_6$ octahedron in the 2D LDH layers. Theoretical calculations have predicted that the binding energy of ZnAl-LDH is higher than that of MgAl-LDH, a difference which leads to a lower carrier binding capacity for the MgAl-LDH host layers. The transfer characteristics of the as-fabricated devices were also characterized. Figure 2d shows the I_d–V_g curve of the Mg-Al-CO$_3$-LDH, which exhibits a distinctive downward trend over the increase of V_g. This suggests a hole conduction of the LDH and that the concentration of charge carriers in the channel are tuned slightly over changes in the gate voltage. Based on the transfer characteristics as well as the standard parallel plate capacitor model, the carrier mobility can be expressed as follows

$$\mu = \frac{L}{WC_iV_{sd}}\frac{\partial I_{sd}}{\partial V_g} \tag{1}$$

where μ is the carrier mobility, L is the channel length (1.0 μm), W is the channel width (8.0 μm), and C_i is the capacitance between the channel and the back gate per unit area, (1.17 × 10^{-4} F m^{-2}: $C_i = \varepsilon_0\varepsilon_r/d$, $\varepsilon_r = 3.9$, $d = 300$ nm). From the data presented in Figure 2d, the carrier mobility of the MgAl-CO$_3$-LDH devices was calculated to be 1.07 × 10^{-5} cm^2 V^{-1} s^{-1}, a result comparable to organic C$_{60}$-based FET devices previously studied.[41] In addition, attempts were made to also measure the output characteristic curves at various gate voltages; however the devices did not allow for sufficient current control to obtain reliable output data.

According to previous research,[42] the electric conductivity of LDH-based crystalline materials may be influenced by the guest anions in the interlayer region. For this reason, a third LDH with a different interlayer guest, MgAl-NO$_3$-LDH, was fabricated to further compare the electronic conductivities. The MgAl-NO$_3$-LDH microcrystals were prepared by treating the previously prepared MgAl-CO$_3$-LDH samples with a salt–acid mixed solution that led to the deintercalation of the carbonate ions and subsequent anion exchange. **Figure 3**a shows typical XRD patterns of these two LDH. In the case of the MgAl-NO$_3$-LDH, the 003 and 006 reflections with d values corresponding to interlayer spacing of 0.75 and 0.375 nm for the MgAl-CO$_3$-LDH have disappeared, and a new series of intense basal reflections at lower 2θ angles (ca. 10°, d ≈ 0.78 nm) have appeared. The larger basal spacing for the NO$_3$-LDH can be attributed to a decrease in the host–guest interaction
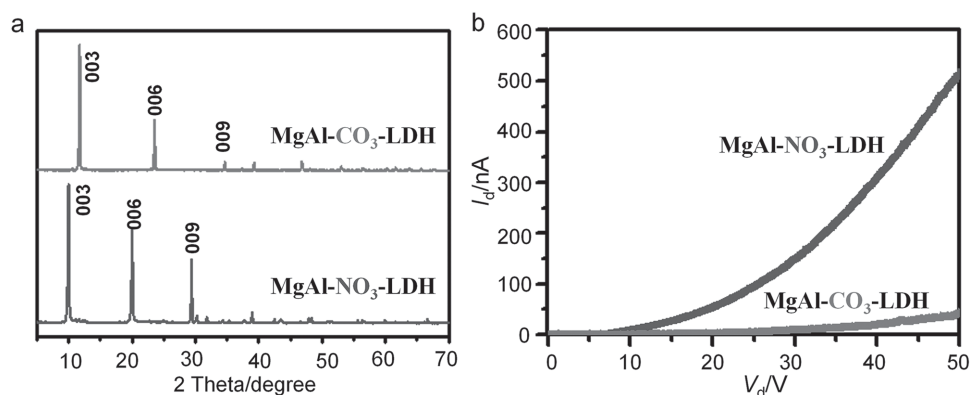
Figure 3. a) XRD patterns of MgAl-CO$_3$-LDH and MgAl-NO$_3$-LDH solids. b) I_d–V_d curves of MgAl-CO$_3$-LDH and MgAl-NO$_3$-LDH based FETs, V_g = 0 V.

between the LDH layers and NO$_3^-$ ions.[43,44] The electric conductivities of the LDH containing different anions in the interlayer region were also studied. The measured I–V curves are shown in Figure 3b, and show that the electric conductivity of the NO$_3$-LDH-based prototype device has hugely increased compared with the CO$_3$-LDH. Given this result, the properties of these two LDH materials were carefully compared to determine the origin of the large differences in electric conductivity. In NO$_3$-LDH, binding forces between the host LDH layer and NO$_3^-$ (such as electrostatic and hydrogen bonding interactions) are much smaller than those in CO$_3$-LDH, a fact illustrated by the different interlayer spacing between the LDH layers, and which is beneficial to the mobility of the carriers. The carrier mobility of the MgAl-NO$_3$-LDH devices was calculated to be 9.30×10^{-5} cm^2 V^{-1} s^{-1}. In additional tests, the electric conductivities of ZnAl-CO$_3$-LDH and ZnAl-NO$_3$-LDH were compared and showed a similar trend (Figure S2, Supporting Information): with carrier mobility values estimated as 1.06×10^{-6} cm^2 V^{-1} s^{-1} and 1.50×10^{-6} cm^2 V^{-1} s^{-1}, respectively. Based on these results, it can be concluded that the carrier transport properties of LDH are highly tunable through adjustment of the interlayer species.

The way in which the thickness of LDH microcrystals affected electrical conductivities was also examined. This relationship has proven highly significant for the electric properties for other 2D materials as the ratio of surface charges and

bulk charges has determined the tunability of the material for FET devices.[45] First, MgAl-NO$_3$-LDH crystals samples were exfoliated into ultrathin nanosheets with thicknesses of 15 and 5 nm.[46] Sample morphologies and thicknesses were confirmed using AFM (Figure S3, Supporting Information) after which FETs were fabricated based on these nanosheets. **Figure 4**a shows the I–V characteristics of both 5 and 15 nm thick LDH sheets. When compared with the results of the 260 nm thick crystals (Figure 3b), it was obvious that the conductivity of LDH crystals decreased rapidly with the decrease in thickness. For example, for a value of V_{ds} = 30 V, the I_{ds} of the 15 nm thick LDH was about six times that of the 5 nm thick LDH, while the value of the 260 nm thick LDH was about 900 times that of the 5 nm thick LDH. This phenomenon is also consistent with the conductive mechanism mentioned above, in which holes at the layers are the main carriers. The thinner LDH layers contain much fewer carriers, and so conductivity is also smaller. In addition, the transfer characteristic curves of these ultrathin LDH were also measured, as shown in Figure 4b. The gate tunability of the LDH crystals decreased as the thickness decreased. This effect is due to the fact that in the case of the ultrathin LDH nanosheets, the number of anions surrounding the host layer board is relatively larger, leading a stronger binding force between the carriers and the host layer board.[41]

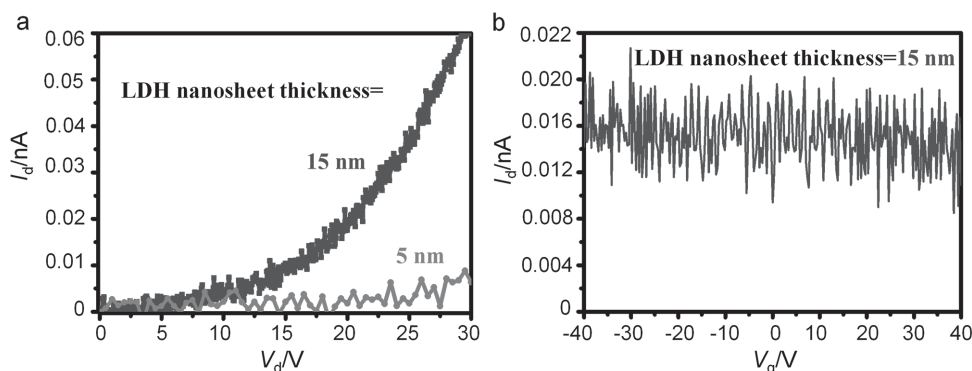In conclusion, microsized and monodispersed 2D LDH microcrystals have been prepared based on a modified

Figure 4. a) I_d–V_d curves of MgAl-LDH nanosheets based FETs with differing thicknesses. b) I_d–V_g curve of LDH microsheet based FET with thickness of 15 nm, V_d = 20 V.

hydrothermal method. These sheet-like structures were successfully used to fabricate electronic devices. Electrical transport studies confirmed that the conductivities of 2D LDH micro/nanostructures can be tuned to ≈100 times their original magnitude through the adjustment of the chemical components of host layers and interlayer guests, as well as the thickness of the LDH microsheets. The carrier mobility of MgAl-NO_3-LDH reached 9×10^{-5} cm^2 V^{-1} s^{-1}. This work not only reported the conductivity characteristics of typical LDH materials at the single crystal level, but also confirmed that the electrical properties of 2D LDH are highly tunable. Due to the wide maneuverability, ease of exchanging guest anions, and delamination properties of LDH, it can be expected that many potential functional molecules will be assembled into the interlayer of 2D materials in order to fabricate prototype devices for future applications in electrical, optical, and magnetic fields.

Experimental Section

Synthesis of LDH Microcrystals: M^{II}Al-CO_3-LDH was synthesized using a modified synthesis method carried out in a two-neck flask equipped with a reflux condenser under a continuous nitrogen flow. A typical procedure progressed as follows: 0.1 mol M^{II}(NO_3)•6H_2O (where M^{II} = Mg^{2+}, Zn^{2+}), 0.05 mol of Al(NO_3)$_3$•6H_2O, and 0.6 mol urea were dissolved in 300 mL deionized water. The mixed solution was then heated at a reflux temperature of 100 °C for 20 h. The resulting solid product was filtered, washed several times with deionized water and anhydrous ethanol, and finally air-dried at 70 °C for 12 h. The M^{II}Al-NO_3-LDH was then prepared by treating M^{II}Al-CO_3-LDH with a salt–acid mixed solution that led to deintercalation of the carbonate ions. Specifically, the LDH sample was dispersed into aqueous solution containing $NaNO_3$ and HNO_3. After purging with nitrogen gas, the vessel was sealed, then shaken for 48 h at ambient temperature. The exchanged product was isolated using the same procedure as was described for the original material.

Exfoliation of LDH Crystals: LDH crystals (0.1 g) were mixed with 100 mL of formamide in a conical beaker, purged with nitrogen gas, and tightly capped. The mixture was then agitated vigorously at 160 rpm in a mechanical shaker for 2 d. The resulting pink, translucent colloidal suspension was further treated by centrifugation at 2000 rpm for 10 min in order to remove unexfoliated particles.

Characterization: XRD data were recorded using a Rigaku Rint-2000 diffractometer equipped with graphite monochromatized Cu Kα radiation capabilities ($\lambda = 0.15406$ nm). The shape and size of the LDH crystals were studied using an SEM instrument (Nova NanoSEM 430) operating at 3 kV in secondary electron mode. TEM and SAED characterizations were performed using a Tecnai G2 F20 U-TWIN transmission electron microscope at an acceleration voltage of 300 kV. Finally, a Seiko SPA 400 AFM system was used to examine the surface topography of films deposited on Si wafers.

Device Fabrication and Electric Measurements: The as-prepared LDH microcrystals were first dispersed onto a SiO$_2$/Si substrate and spin-coated with a PMMA photoresist, following which an EBL process was used to define electrode patterns on selected crystals. After pattern development in 1:3 Methyl Isobutyl Ketone (MIBK): Isopropyl

Alcohol (IPA), 300 nm Au/2 nm Ti were deposited onto the device using electron beam evaporation, following which a standard metal lift-off technique was carried out in order to define the electrode patterns. Current–voltage (I–V) characteristics were measured using an Agilent B1500A semiconductor analyzer and a Desert Cryogenics probe station. Bias voltage measurements were performed by applying fixed source–drain (V_{ds}) and source–gate (V_g) voltages while continuously measuring the source–drain current (I_{ds}).

Supporting Information

Supporting information is available from the Wiley Online Library or from the author.

Acknowledgements

[1] L. K. Li, Y. J. Yu, G. J. Ye, Q. Q. Ge, X. D. Ou, H. Wu, D. L. Feng, X. H. Chen, Y. B. Zhang, *Nat. Nanotechnol.* 2014, *9*, 372.

[2] K. S. Novoselov, A. K. Geim, S. V. Morozov, D. Jiang, M. I. Katsnelson, I. V. Grigorieva, S. V. Dubonos, A. A. Firsov, *Nature* 2005, *438*, 197.

[3] F. N. Xia, H. Wang, D. Xiao, M. Dubey, A. Ramasubramaniam, *Nat. Photonics* 2014, *8*, 899.

[4] L. Britnell, R. M. Ribeiro, A. Eckmann, R. Jalil, B. D. Belle, A. Mishchenko, Y. J. Kim, R. V. Gorbachev, T. Georgiou, S. V. Morozov, A. N. Grigorenko, A. K. Geim, C. Casiraghi, A. H. Castro Neto, K. S. Novoselov, *Science* 2013, *340*, 1311.

[5] A. K. Geim, I. V. Grigorieva, *Nature* 2013, *499*, 419.

[6] T. Georgiou, R. Jalil, B. D. Belle, L. Britnell, R. V. Gorbachev, S. V. Morozov, Y. J. Kim, A. Gholinia, S. J. Haigh, O. Makarovsky, L. Eaves, L. A. Ponomarenko, A. K. Geim, K. S. Novoselov, A. Mishchenko, *Nat. Nanotechnol.* 2013, *8*, 100.

[7] X. P. Hong, J. Kim, S. F. Shi, Y. Zhang, C. H. Jin, Y. H. Sun, S. Tongay, J. Q. Wu, Y. F. Zhang, F. Wang, *Nat. Nanotechnol.* 2014, *9*, 682.

[8] A. Pospischil, M. M. Furchi, T. Mueller, *Nat. Nanotechnol.* 2014, *9*, 257.

[9] J. S. Ross, P. Klement, A. M. Jones, N. J. Ghimire, J. Q. Yan, D. G. Mandrus, T. Taniguchi, K. Watanabe, K. Kitamura, W. Yao, D. H. Cobden, X. D. Xu, *Nat. Nanotechnol.* 2014, *9*, 268.

[10] F. Withers, O. Del Pozo-Zamudio, A. Mishchenko, A. P. Rooney, A. Gholinia, K. Watanabe, T. Taniguchi, S. J. Haigh, A. K. Geim, A. I. Tartakovskii, K. S. Novoselov, *Nat. Mater.* 2015, *14*, 301.

[11] X. Yang, F. Zhai, H. Hu, D. Hu, R. Liu, S. Zhang, M. Sun, Z. Sun, J. Chen, Q. Dai, *Adv. Mater.* 2016, *28*, 2931.

[12] H. T. Yuan, X. G. Liu, F. Afshinmanesh, W. Li, G. Xu, J. Sun, B. Lian, A. G. Curto, G. J. Ye, Y. Hikita, Z. X. Shen, S. C. Zhang, X. H. Chen, M. Brongersma, H. Y. Hwang, Y. Cui, *Nat. Nanotechnol.* 2015, *10*, 707.

[13] M. Buscema, D. J. Groenendijk, G. A. Steele, H. S. J. van der Zant, A. Castellanos-Gomez, *Nat. Commun.* 2014, *5*, 6.

[14] K. K. Kim, A. Hsu, X. T. Jia, S. M. Kim, Y. S. Shi, M. Hofmann, D. Nezich, J. F. Rodriguez-Nieva, M. Dresselhaus, T. Palacios, J. Kong, *Nano Lett.* **2012**, *12*, 161.

[15] K. S. Novoselov, A. K. Geim, S. V. Morozov, D. Jiang, Y. Zhang, S. V. Dubonos, I. V. Grigorieva, A. A. Firsov, *Science* **2004**, *306*, 666.

[16] Y. J. Zhan, Z. Liu, S. Najmaei, P. M. Ajayan, J. Lou, *Small* **2012**, *8*, 966.

[17] J. Maier, *Nat. Mater.* **2005**, *4*, 805.

[18] R. Waser, M. Aono, *Nat. Mater.* **2007**, *6*, 833.

[19] A. I. Khan, D. O'Hare, *J. Mater. Chem.* **2002**, *12*, 3191.

[20] R. Z. Ma, T. Sasaki, *Adv. Mater.* **2010**, *22*, 5082.

[21] V. Rives, M. A. Ulibarri, *Coord. Chem. Rev.* **1999**, *181*, 61.

[22] B. Li, Y. F. Zhao, S. T. Zhang, W. Gao, M. Wei, *ACS Appl. Mater. Interfaces* **2013**, *5*, 10233.

[23] Z. P. Liu, R. Z. Ma, M. Osada, N. Iyi, Y. Ebina, K. Takada, T. Sasaki, *J. Am. Chem. Soc.* **2006**, *128*, 4872.

[24] D. P. Yan, J. Lu, J. Ma, M. Wei, D. G. Evans, X. Duan, *Angew. Chem. Int. Ed.* **2011**, *50*, 720.

[25] D. P. Yan, J. Lu, M. Wei, J. B. Han, J. Ma, F. Li, D. G. Evans, X. Duan, *Angew. Chem. Int. Ed.* **2009**, *48*, 3073.

[26] D. G. Evans, X. Duan, *Chem. Commun.* **2006**, *7*, 485.

[27] Y. W. Liu, H. Cheng, M. J. Lyu, S. J. Fan, Q. H. Liu, W. S. Zhang, Y. D. Zhi, C. M. Wang, C. Xiao, S. Q. Wei, B. J. Ye, Y. Xie, *J. Am. Chem. Soc.* **2014**, *136*, 15670.

[28] B. Sels, D. De Vos, M. Buntinx, F. Pierard, A. Kirsch-De Mesmaeker, P. Jacobs, *Nature* **1999**, *400*, 855.

[29] M. F. Shao, F. Y. Ning, Y. F. Zhao, J. W. Zhao, M. Wei, D. G. Evans, X. Duan, *Chem. Mater.* **2012**, *24*, 1192.

[30] J. Wang, K. Li, H. X. Zhong, D. Xu, Z. L. Wang, Z. Jiang, Z. J. Wu, X. B. Zhang, *Angew. Chem., Int. Ed.* **2015**, *54*, 10530.

[31] J. W. Zhao, J. Chen, S. M. Xu, M. F. Shao, Q. Zhang, F. Wei, J. Ma, M. Wei, D. G. Evans, X. Duan, *Adv. Funct. Mater.* **2014**, *24*, 2938.

[32] J. A. Gursky, S. D. Blough, C. Luna, C. Gomez, A. N. Luevano, E. A. Gardner, *J. Am. Chem. Soc.* **2006**, *128*, 8376.

[33] Y. Chen, D. P. Yan, Y. F. Song, *Dalton Trans.* **2014**, *43*, 14570.

[34] J. B. Liang, R. Z. Ma, N. B. O. Iyi, Y. Ebina, K. Takada, T. Sasaki, *Chem. Mater.* **2010**, *22*, 371.

[35] C. Chakraborty, K. Dana, S. Malik, *J. Phys. Chem. C* **2011**, *115*, 1996.

[36] A. I. Khan, D. O'Hare, *J. Mater. Chem.* **2002**, *12*, 3191.

[37] T. S. Stanimirova, G. Kirov, E. Dinolova, *Mater. Sci. Lett.* **2001**, *20*, 453.

[38] X. Duan, D. G. Evans, *Layered Double Hydroxides*, Springer, Berlin, Germany **2006**.

[39] H. Yan, M. Wei, J. Ma, D. G. Evans, X. Duan, *J. Phys. Chem. A* **2010**, *114*, 7369.

[40] Z. Liu, R. Ma, M. Osada, N. Iyi, Y. Ebina, K. Takada, T. Sasaki, *J. Am. Chem. Soc.* **2006**, *128*, 4872.

[41] T. Wakahara, P. D'Angelo, K. I. Miyazawa, Y. Nemoto, O. Ito, N. Tanigaki, D. D. C. Bradley, T. D. Anthopoulos, *J. Am. Chem. Soc.* **2012**, *134*, 7204.

[42] X. X. Guo, F. Z. Zhang, D. G. Evans, X. Duan, *Chem. Commun.* **2010**, *46*, 5197.

[43] Z. P. Liu, R. Z. Ma, Y. Ebina, N. Iyi, K. Takada, T. Sasaki, *Langmuir* **2007**, *23*, 861.

[44] R. Z. Ma, Z. P. Liu, L. Li, N. Iyi, T. Sasaki, *J. Mater. Chem.* **2006**, *16*, 3809.

[45] B. Radisavljevic, A. Radenovic, J. Brivio, V. Giacometti, A. Kis, *Nat. Nanotechnol.* **2011**, *6*, 147.

[46] Z. Liu, R. Ma, Y. Ebina, N. Iyi, K. Takada, T. Sasaki, *Langmuir* **2007**, *23*, 861.